Title

Cytochrome P450 125A4, the Third Cholesterol C-26 Hydroxylase from Mycobacterium smegmatis

Permalink

https://escholarship.org/uc/item/95q894rp

Journal

Biochemistry, 54(46)

ISSN

0006-2960

Authors

Frank, Daniel J
Waddling, Christopher A
La, Maggie
et al.

Publication Date

2015-11-24

DOI

10.1021/acs.biochem.5b01029

Peer reviewed

BIOCHEMISTRY

including biophysical chemistry & molecular biology

Cytochrome P450 125A4, the Third Cholesterol C-26 Hydroxylase from *Mycobacterium smegmatis*

Daniel J. Frank,[†] Christopher A. Waddling,[‡] Maggie La,[†] and Paul R. Ortiz de Montellano*[,†]

[†]Department of Pharmaceutical Chemistry, University of California, San Francisco, California 94158-2517, United States
[‡]Department of Biochemistry and Biophysics, University of California, San Francisco, California 94158-2517, United States

ABSTRACT: *Mycobacterium tuberculosis* (*Mtb*) and *Mycobacterium smegmatis* (*Msmeg*) can grow on cholesterol as the sole carbon source. In *Mtb* the utilization of cholesterol can be initiated by CYP125A1 or CYP142A1 and in *Msmeg* by the orthologous CYP125A3 and CYP142A2. Double knockout of the two enzymes in *Mtb* prevents its growth on cholesterol, but the double knockout of *Msmeg* is still able to grow, albeit at a slower rate. We report here that *Msmeg* has a third enzyme, CYP125A4, that also oxidizes cholesterol, although it has a much higher activity for the oxidation of 7α-hydroxycholesterol. The ability of *Msmeg* CYP125A4 (and *Mtb* CYP125A1) to oxidize 7α-hydroxycholesterol is due, at least in part, to the presence of a smaller amino acid side chain facing C-7 of the sterol substrate than in CYP125A3. The ability to oxidize 7-substituted steroids broadens the range of sterol carbon sources for growth, but even more importantly in *Mtb*, additional biological effects are possible due to the potent immunomodulatory activity of 7α,26-dihydroxycholesterol.
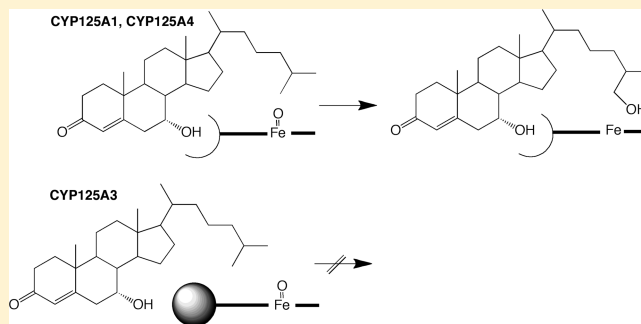
Mycobacterium tuberculosis (*Mtb*) is the causative agent of tuberculosis, a disease that the World Health Organization estimates kills 1.3 million people annually.[1,2] During infection, *Mtb* takes up residence in the phagosomes of host macrophages. To survive and replicate in this nutritionally poor environment, *Mtb* has evolved pathways to utilize host-derived nutrients. Cholesterol is one such abundant intracellular molecule that *Mtb* can import and degrade either for energy or as a biosynthetic precursor.[1,2] Disruption of the cholesterol metabolic pathway leads to attenuation in models of infection and loss of the ability to grow *in vitro* on cholesterol as a sole carbon source, clearly indicating the importance of the availability of cholesterol to the intracellular viability of the pathogen as well as the potential for targeting this pathway for the development of novel therapeutic agents.[1,3−6] The first and enabling step in the cholesterol degradation pathway is the oxidation of the cholesterol alkyl side chain to a carboxylic acid by cytochromes P450 (CYP) 125A1 (*Rv3545c*) and 142A1 (*Rv3518c*), which can then be further catabolized via a β-oxidation pathway.[7−9] This pathway is conserved in *Rhodococcus jostii*,[10] as well as *Mycobacterium smegmatis* (*Msmeg*), a soil-dwelling nonpathogenic relative of *Mtb*, where it is under the control of the TetR-like repressor KstR. In *Msmeg*, CYP125A3 (*MSMEG_5995*) and CYP142A2 (*MSMEG_5918*) serve as orthologs for the oxidation of cholesterol at C-26.[11−13] However, unlike its *Mtb* relative, the *Msmeg* Δ*cyp125a3*/Δ*cyp142a2* double mutant retains its ability to utilize cholesterol as a carbon source for growth *in vitro*.[14]

To investigate this difference in cholesterol metabolism, we first examined CYP189A1 (*MSMEG_4829*), a cytochrome P450 of unknown function, previously shown to be upregulated

in response to cholesterol, although not under direct control of the KstR regulatory pathway.[15] However, as reported here, *in vitro* binding and oxidation assays failed to show any activity for this enzyme toward cholesterol, 4-cholesten-3-one, or other structurally related compounds. Our attention then turned to CYP125A4 (*MSMEG_3524*), a gene not observed to be upregulated in response to cholesterol but that shares approximately 65% sequence identity with CYP125A3. Surprisingly, CYP125A4 showed only weak activity toward cholesterol and 4-cholesten-3-one *in vitro*, but it had robust activity toward 7α-hydroxy-4-cholesten-3-one, forming 7α,26-dihydroxy-4-cholesten-3-one, a compound implicated in immune cell migration and signaling in humans.[16,17] In contrast, CYP125A3 failed to show any activity toward this oxysterol.

Homology modeling of CYP125A3 and CYP125A4 using the CYP125A1 structure in complex with its substrate 4-cholesten-3-one [Protein Data Bank (PDB) entry 2X5W], as opposed to CYP125A3 where only the ligand free structure is available, revealed a single amino acid difference near the cholesterol C-7 position. A bulkier Trp83 in CYP125A3, compared to the corresponding Tyr87 in CYP125A4 (or Phe100 in CYP125A1), protrudes farther into the active site cavity, possibly acting as a steric block to binding of the 7α-substituted oxysterol. Site-directed mutagenesis of the two enzymes to generate the mutants CYP125A3 W83Y and CYP125A4 Y87W resulted in

enzymes that effectively reversed their substrate profiles, albeit with reduced activity relative to that of the wild-type enzymes. A crystal structure of the CYP125A3 W83Y mutant revealed an enlarged active site relative to that of the wild-type enzyme that provides easier access of the 7α-substituted oxysterol to the active site in the mutant enzyme.

This study highlights a subtle difference in the cholesterol metabolic pathways of these two mycobacterial species, which is relevant to the consideration of *Msmeg* as a model system for the development of therapeutic agents against the *Mtb* pathway.

■ EXPERIMENTAL PROCEDURES

Chemicals. 1,4-Cholestadiene-3-one was obtained from Research Plus (Barnegat, NJ), and 7α-hydroxycholesterol and 7α-hydroxy-4-cholesten-3-one were from Avanti Polar Lipids (Alabaster, AL). All other chemicals, including cholesterol, spinach ferredoxin, spinach ferredoxin-NADP$^+$-reductase, bovine liver catalase, glucose 6-phosphate, glucose-6-phosphate dehydrogenase, and methyl-β-cyclodextrin, were purchased from Sigma-Aldrich (St. Louis, MO).

Protein Cloning and Mutagenesis. *MSMEG_4829* (CYP189A1) and *MSMEG_3524* (CYP125A4) were amplified by polymerase chain reaction using Pfu Turbo DNA polymerase (New England BioLabs), primer pairs 5′-TTTTTTCAT-ATGGCCCAGCCCAGCACCAGTGC and 5′-AAAAAAAAG-CTTATTATTAGTGATGGTGATGGTGATGGCGCACGA-ACGTTGGCATG (CYP189A1), and 5′-TTTTTTCATATGGTGGTCATGAGCGATAGTGC and 5′-AAAAAAAAGCTATTATTAGTGATGGTGATGGTGATGT-CGATCTGCCTGCGACGAC (CYP125A4), and genomic DNA from *M. smegmatis* mc^{2}155 as a template. The resulting DNA fragments were digested using *Nde*I and *Hin*dIII (New England BioLabs) and cloned into the *pCWOri+* vector.[18] The expression vector used for expression of the CYP125A3 and 125A4 mutants was constructed by amplification of the modified gene coding sequence from an existing *pCWori/cyp125A4* vector generated for this study or the *pCWori/cyp125A3* vector described previously.[14] As per the instructions of the QuikChange Lightning Site Directed Mutagenesis Kit (Agilent), 2 μL of *Dpn*I restriction enzyme was added to digest the parental supercoiled dsDNA and transformed in XL-10 ultracompetent cells. The resulting plasmid was purified and digested using *Nde*I and *Hin*dIII and ligated into a similarly digested *pCWori+* vector to provide the mutant expression vector. Primers used to generate CYP125A3 W83Y were 5′-GTCCTGCGGATACACCGGGATGGCGCCG and 5′-CGG-CGCCATCCCGGTGTCCGCAGGAC and CYP125A4 Y87W 5′-GTCCCTTCGGGCCAACGCGGCAGCGCGGGT and 5′-ACCGCGCTGCCGCGTTGGCCCGAAGGGAC. The enzyme coding region of the mutant expression vector was sequenced for accuracy (Elim Biopharmaceuticals, Hayward, CA).

Protein Expression, Purification, and Homology Modeling. CYPs 189A1, 125A1, 125A3, 125A4, 125A3 W83Y, and 125A4 Y87W were expressed and purified as previously described,[14,19] with the exception of CYP125A4 Y87W, which was expressed under the same conditions with the addition of the co-expression chaperone plasmid *pTGroE* and in the presence of 20 μg/mL kanamycin.[20] Briefly, *Escherichia coli* DH5α cells containing the *pCWori* expression vector with the gene of interest were grown at 37 °C and 250 rpm in TB medium containing 100 μg/mL ampicillin until an OD$_{600}$ of 0.7−0.8 was achieved. Expression of the proteins was induced by the addition of 1 mM isopropyl β-D-1-thiogalactopyranoside and 0.5 mM δ-aminolevulinic acid, and the culture was continued for 36 h at 25 °C and 180 rpm. Cultures were harvested by centrifugation and stored at −80 °C. Cell pellets were thawed on ice and resuspended in 50 mM Tris-HCl (pH 7.4), 0.15 M NaCl, and 1 mM phenyl-methanesulfonyl fluoride with agitation before the addition of 0.5 mg/mL lysozyme and 0.1 mg/mL DNase. The cells were disrupted by sonication using a Branson sonicator (six cycles of 1 min followed by 30 s rests), clarified by centrifugation at 100000g for 45 min at 4 °C, purified on a Ni-NTA column, washed with 10 column volumes of resuspension buffer and 20 mM imidazole, and eluted with resuspension buffer and 250 mM imidazole. Elution fractions were concentrated and dialyzed against 50 mM Tris-HCl (pH 7.4), and the concentration was determined from difference spectra using an extinction coefficient of 91000 M^{-1} cm^{-1}.[21] The fraction of P420 species never exceeded 5%. Molecular models for CYP 125A3 and 125A4 were generated using MODELER[22] with the structure of CYP125A1 in complex with 4-cholesten-3-one (PDB entry 2X5W) as the template. For crystallography, proteins were further purified by flow-through chromatography on SP-Sepharose Fast-Flow (Amersham Biosciences) and subsequent binding to Q-Sepharose Fast-Flow (Amersham Biosciences), both equilibrated with 50 mM Tris-HCl buffer (pH 7.5), and washed with 5 column volumes of equilibration buffer. After being washed, the proteins were eluted with 0.5 M NaCl in 50 mM Tris-HCl (pH 7.5). The protein was then buffer exchanged into 50 mM potassium phosphate (pH 7.4).

Crystallization, Data Collection, and Model Refinement. Single crystals of CYP124A3 W83Y were grown via hanging-drop vapor diffusion in drops containing 100 nL of a protein solution and 100 nL of a precipitant solution. The well over which the crystals grew contained 0.1 M phosphate-citrate buffer at pH 4.2 and 40% (v/v) PEG 600. To the protein solution in the crystallization drop were added 90 nL of the well solution and 10 nL of additive screen containing 0.33% (w/v) 2,6-naphthalenedisulfonic acid disodium salt, 0.33% (w/v) 2-aminobenezesulfonic acid, and 0.33% (w/v) *m*-benzene-disulfonic acid disodium salt, and 0.02 M HEPES sodium at pH 6.8. Reddish-brown cube-shaped crystals grew within 14 days at 20 °C.

Data were collected at Advanced Light Source beamline 8.3.1 on a single crystal with approximate dimensions of 65 μm × 65 μm × 50 μm; 200 nL of 100% PEG 400 was added to the drop containing the crystal, and the resultant drop was allowed to sit for 1 min, after which time the crystal was pulled from the drop and mounted directly in the cryostream. Two data sets were collected, the first a low-resolution set at 1 s exposures, followed by a second high-resolution set at 3 s per exposure, and were processed at the beamline using Elves.[23−26] Table 1 lists the relevant data collection and structure refinement statistics.

The structure was determined by molecular replacement in Phenix[27] using a water and ligand free model of the previously determined 2.0 Å structure of CYP125A3 (PDB entry 4APY). Rigid body refinement was followed by the addition of the protoporphyrin IX containing Fe and water molecules. TLS refinement[28] was performed using four groups: residues 2−119, 120−144, 145−280, and 281−411. Phosphate and citrate ions were added to appropriately sized regions of positive electron density. Several atoms of PEG 600 were added to clear positive density in a position that indicated it was bound to the Fe(II)

Table 1. Data and Structure Refinement Statistics

Data Collection	
space group	$I4_1$
unit cell [a, c (Å)]	108.566, 118.715
limiting resolution (Å)	2.262
total no. of reflections	63505
no. of unique reflections	32185
$I/(I)$	19.37
completeness (%)	99.67
R_{merge} (Å)	4.274 (52.72)
Structure Refinement	
resolution range (Å)	80.25–2.262
R_{work}	0.1646 (0.3166)
R_{free}	0.2088 (0.3460)
root-mean-square deviation for bond lengths (Å)	0.004
root-mean-square deviation for bond angles (deg)	0.80
no. of protein residues	410
no. of waters	86
no. of ligand atoms	86
average isotropic B factor (Å^2)	
protein atoms	63.3
solvent atoms	57.3
ligand atoms	70.6

of the protoporphyrin IX and located within the cholesterol binding pocket. Coordinates for this structure can be found in the Protein Data Bank (entry 5DQN).

UV−Visible (UV−vis) Spectroscopy. UV−visible absorption spectra were recorded on a Cary UV−visible scanning spectrophotometer (Varian) using a 1 cm path-length quartz cuvette at ambient temperature in 50 mM potassium phosphate buffer (pH 7.4) containing 150 mM NaCl. Spectral titrations were performed using 3 μM P450 with the sequential addition of substrates from concentrated stocks in methanol, with the same solution added to the reference cuvette. Difference spectra were recorded from 250 to 750 nm at a scanning rate of 120 nm/min. Data were fitted to a quadratic equation (eq 1) or a Hill equation (eq 2) using GraphPad Prism

$$A_{obs} = A_{max}\{[S] + [Et] + K_S - [([S] + [Et] + K_S)^2 - (4[S][Et])]^{0.5}\}/2[Et] \quad (1)$$

$$A_{obs} = A_{max} \times [S]^n / S_{50}{}^n + [S]^n \quad (2)$$

where A_{obs} is the observed absorption shift, A_{max} is the maximal shift, K_S (or S_{50} for the Hill equation) is the apparent dissociation constant, [Et] is the total enzyme concentration, [S] is the ligand concentration, and n is the Hill coefficient. Assays were completed in triplicate, and error bars represent the standard error.

Steady-State Kinetic Studies and Product Analysis. Enzymes (0.5 or 3 μM) were preincubated for 5 min at ambient temperature with substrate in 50 mM potassium phosphate (pH 7.4) containing 0.05% (w/v) methyl-β-cyclodextrin, 150 mM NaCl, and 10 mM MgCl$_2$. Reactions were initiated by adding 100 mM NADPH, 1 μM spinach ferredoxin, 0.2 unit mL^{-1} spinach ferredoxin-NADP$^+$ reductase, 0.1 mg mL^{-1} bovine liver catalase, and an NADPH-regenerating system consisting of 0.4 unit mL^{-1} glucose-6-phosphate dehydrogenase and 5 mM glucose 6-phosphate. Aliquots of 50 μL were taken between 0 and 30 min and quenched with 150 μL of acetonitrile containing 0.1% formic acid (FA) and 10 μM 1,4-cholestadiene-3-one as an internal standard. The reaction

mixtures were centrifuged at 10000g for 4 min. Product formation was found to be linear with protein concentration and reaction time. For reactions with cholesterol or 7α-hydroxycholesterol, reactions were allowed to proceed for 45 min at ambient temperature, followed by the addition of 1 μL of cholesterol oxidase (1 UN/μL) and incubation for an additional 45 min at ambient temperature before analysis.

For quantification of the products, the reactions were analyzed by high-performance liquid chromatography (HPLC) using an Agilent Series 1200 HPLC system and a reverse phase C18 column (Waters Xterra C18, 3.5 μm, 2.1 mm × 50 mm). For the 4-cholesten-3-one and cholesterol reactions, the samples were eluted isocratically at a flow rate of 0.5 mL/min (solvent A, H$_2$O and 0.1% formic acid; solvent B, CH$_3$CN and 0.1% formic acid) with a gradient starting at 70% B for 1 min and the solvents ramped to 100% B over 11 min. The elution was maintained at 100% B until 14 min and then ramped back to 70% B within 1 min, followed by equilibration at the same composition for 2 min before the next run. The elution was monitored at 240 nm. For the 7α-hydroxy-4-cholesten-3-one and 7α-hydroxycholesterol reactions, the samples were eluted isocratically at a flow rate of 0.5 mL/min (solvent A, H$_2$O and 0.1% formic acid; solvent B, CH$_3$CN and 0.1% formic acid) with a gradient starting at 5% B for 3 min and the solvents ramped to 95% B over 11 min. The elution was maintained at 95% B until 16 min and then ramped back to 5% B within 0.1 min, followed by equilibration for 6 min. The elution was monitored at 240 nm.

To determine the K_M values, the data points were fitted to a quadratic equation (eq 3) or a Hill equation (eq 4) using GraphPad Prism

$$k_{obs} = k_{max}\{[S] + [Et] + K_M - [([S] + [Et] + K_M)^2 - (4[S][Et])]^{0.5}\}/2[Et] \quad (3)$$

$$k_{obs} = k_{max} \times [S]^n / S_{50}{}^n + [S]^n \quad (4)$$

where k_{obs} is the product forming rate determined at any ligand concentration, k_{max} is the maximal rate, K_M (or S_{50} for the Hill equation) is the substrate concentration at which the half-maximal rate is achieved, [Et] is the total enzyme concentration used, [S] is the ligand concentration, and n is the Hill coefficient. Assays were completed in triplicate, and error bars represent the standard error.

■ RESULTS

Spectroscopic Properties of CYP189A1. Previous work from our laboratory revealed the ability of the *Msmeg* $\Delta cyp125a3/\Delta cyp142a2$ double knockout to utilize cholesterol as a carbon source,[14] unlike a similar mutant of *Mtb* that was unable to grow on cholesterol *in vitro*.[6] Microarray analysis of the *Msmeg* mutant showed the presence of a single additional cytochrome P450-encoding gene, *MSMEG_4829* (CYP189A1), that was upregulated in response to cholesterol.[14] With no ortholog in the *Mtb* genome, we hypothesized that CYP189A1 might be responsible for the *Msmeg* double mutant's ability to grow on cholesterol. CYP189A1 was therefore cloned and expressed (see Experimental Procedures) and tested for its ability to oxidize cholesterol. The UV−visible spectrum of the protein was that of a classical, low-spin-state P450 enzyme with a Soret maximum at 419 nm, which shifted to 421 nm in the presence of the type II ligand econazole (Figure 1A). Reduction with sodium dithionite and binding of
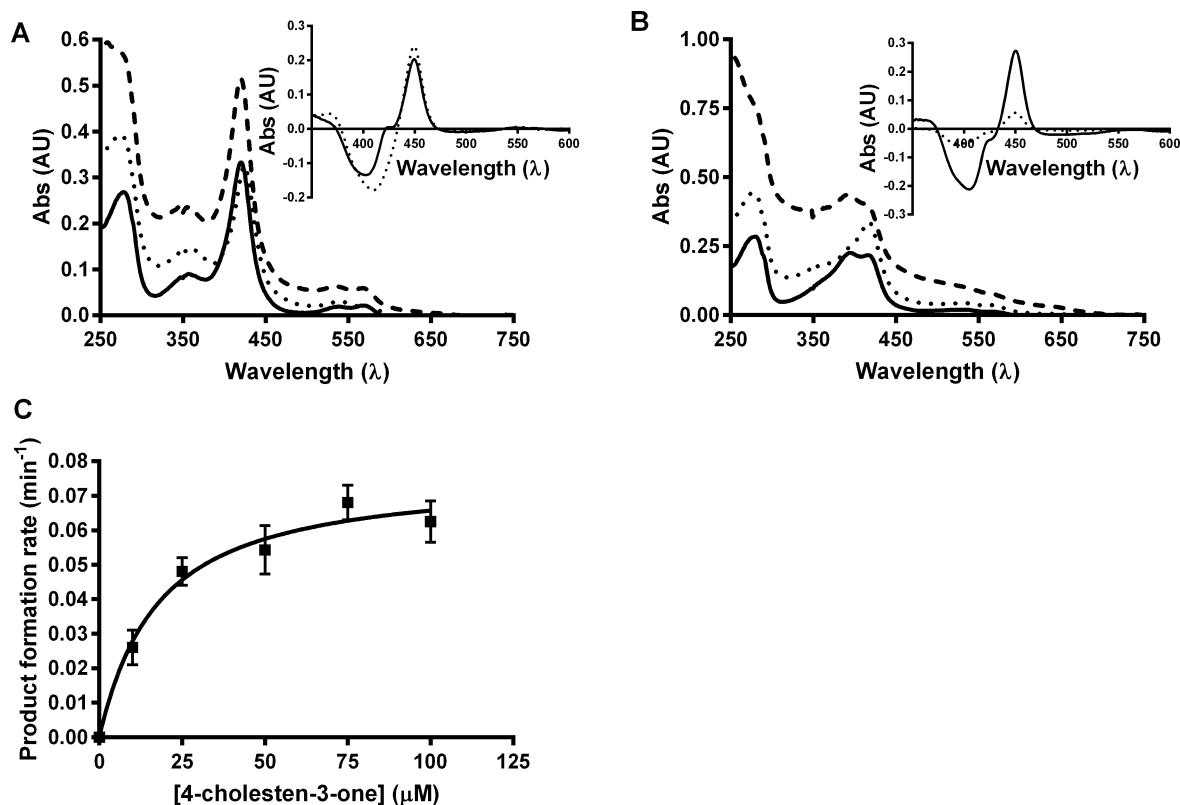
Figure 1. UV−visible spectra for (A) CYP189A1 (3 μM) and (B) CYP125A4 (3 μM) without a ligand (—), with 50 μM 4-cholesten-3-one (———), and with 50 μM econazole (---). The inset shows CO difference spectra after 2 min (---) and 20 min (—). (C) Fit for the CYP125A4 oxidation rate of 4-cholesten-3-one to the quadratic binding equation ($k_{cat}/K_M = 0.002$ μM^{-1} s^{-1}).

carbon monoxide revealed a nearly 100% population of the P450 species, which gradually decayed into the inactive P420 form over the course of 20 min (Figure 1A, inset). However, binding of the proposed substrates cholesterol and 4-cholesten-3-one failed to induce the classical substrate type I binding spectral shift of the Soret peak (Figure 1A), or any other changes in the Soret peak that could be attributed to ligand binding, and oxidation assays revealed no product formation upon incubation of the enzyme with either proposed substrate in the presence of suitable electron donor partners (data not shown). Thus, CYP189A1 is unlikely to be responsible for the *Msmeg* double mutant's residual ability to utilize cholesterol. Additional small molecules, including various terpenes, fatty acids (saturated and unsaturated, single, and branched chain), and polycyclic hydrocarbons, also failed to show any indication of being substrates for this enzyme.

Spectroscopic Properties of CYP125A4 and Oxidation of 4-Cholesten-3-one. Further analysis of the *Msmeg* genome led us to investigate CYP125A4 (*MSMEG_3524*), a gene not upregulated in response to cholesterol but that shares a high degree of sequence homology (>60%) with the CYP125A3 gene (*MSMEG_5995*). Cloning, expression, and purification of *MSMEG_3524* enabled the spectroscopic characterization of CYP125A4, which displayed characteristics similar to those of the previously studied CYP125 enzymes. In the resting state, CYP125A4 was observed to be in a mixture of the low- and high-spin states, characterized by their respective Soret peaks at 414 and 393 nm (Figure 1B), although with a higher fraction of the resting enzyme in the low-spin state than was observed for its homolog CYP125A3.[14] Binding of type II ligand econazole shifted the Soret peak to 421 nm. Reduction of CYP125A4 with

sodium dithionite followed by binding of carbon monoxide revealed a formation of the P450 species slower than that observed with CYP189A1, with a small fraction of the inactive P420 species also being concurrently formed (Figure 1B, inset). The difference is most likely due to slower reduction of the CYP125A4 enzyme by sodium dithionite. These observations are similar to those previously obtained with CYP125A3. Addition of cholesterol or 4-cholesten-3-one did induce a partial shift to the type I high-spin species (Figure 1B), and while both substrates were oxidized to form the C-26 alcohol product, on the basis of the comparison of the product retention time with that of the CYP125A1 reaction product, the overall rate of oxidation by CYP125A4 ($K_M = 15.6 \pm 3.6$ μM; $V_{max} = 0.08 \pm 0.01$ min^{-1}) for 4-cholesten-3-one was approximately 20 times slower than that previously reported for CYP125A3 ($V_{max} = 1.8 \pm 0.1$ min^{-1}) (Figure 1C).[14]

Structural Analysis of CYPs 125A3 and 125A4 and Point Mutants. In search of insight into the reduced activity toward 4-cholesten-3-one observed with CYP125A4, we generated homology models of both CYP125A3 and CYP125A4 using the substrate-bound structure of the *Mtb* ortholog CYP125A1 (PDB entry 2X5W). Although the ligand free structure of CYP125A3 was available as a model, the ligand-bound structure of CYP125A1 revealed conformational changes in the enzyme relative to its ligand free structure, making the ligand-bound *Mtb* ortholog a more suitable model for analyzing protein−ligand interactions.[6] The bulky tryptophan (W83) in the CYP125A3 sequence was observed to be positioned adjacent to C-7 of the 4-cholesten-3-one substrate. In CYP125A4 this residue is replaced with a smaller tyrosine

(Y87) and in the original CYP125A1 structure with a phenylalanine (F100).

Generation of the W83Y mutation in CYP125A3 and determination of the crystal structure (PDB entry 5DQN) showed that the side chain volume change sufficiently increases the size of the binding pocket such that it mimics that found in the CYP125A1 structure 2X5W. This change allows the 7α-hydroxycholesterol ligand greater access to the active site in the mutant than in the wild-type enzyme. Using the discrete volume determination method employed by 3V, the Voss Volume Voxelator,[29] and with the probe radius set to 1.5 Å, the channel volume in the CYP125A3 W83Y structure is found to be enlarged versus that of the wild-type CYP125A3 structure by 32 Å³, 22 Å³ of which can be directly attributed to the smaller tyrosine side chain.[30] Using similar measurement techniques, the 2X5W CYP125A1 structure is found to have a channel volume that is intermediate between those of the two CYP125A3 structures, as shown in Table 2. Alignment of the

Table 2. Binding Pocket Volumes and Contact Statistics

	4APY	5DQN	2X5W
cavity volume (Å³)[a]	2318	2350	2334
contacts (Å)[b]	W83:2.45	Y83:4.03	F100:3.97

[a]Voxel size of 0.5 Å; probe radius of 1.5 Å.[8] [b]Shortest atomic distance to 4-cholesten-3-one in binding position found in 2X5W.

secondary structures of the three proteins using UCSF Chimera[31,32] reinforces the hypothesis that cholesterol faces steric clashes with the tryptophan in wild-type CYP125A3 that are not present in the CYP125A1 structure and would not be seen in the CYP125A3 W83Y mutant. As shown in Figure 2B,[32,33] the bound cholesterol in CYP125A1 structure 2X5W, when modeled into the binding pocket of CYP125A3 structure 4APY, clashes with the Trp83 side chain. When mutated to Tyr83 as in structure 5DQN and shown in Figure 2C, the modeled cholesterol fits much like it does as reported in the 2X5W structure (Figure 2A). Figure 3 illustrates the shape of the binding pocket of the CYP125A3 W83Y mutant, with the ligand 4-cholesten-3-one modeled into the active site.

Binding and Oxidation of 7α-Hydroxysterol Derivatives. To test the impact of this residue on substrate selectivity, we examined the ability of both isoforms to bind 7α-hydroxycholesterol and to oxidize 7α-hydroxy-4-cholesten-3-one. CYP125A3 underwent a sigmoidal reverse type I spin conversion back toward the low-spin species upon binding of 7α-hydroxycholesterol (S_{50} = 32.9 ± 4.7 μM; n = 1.7 ± 0.2) (Figure 4A,B) but failed to oxidize 7α-hydroxy-4-cholesten-3-one. CYP125A4 bound 7α-hydroxycholesterol as a typical type I substrate (K_S = 8.7 ± 0.5 μM) (Figure 4C,D) and readily oxidized 7α-hydroxy-4-cholesten-3-one (K_M = 4.1 ± 1.2 μM; V_{max} = 0.39 ± 0.02 min^{-1}) at rates much higher than the rates with 4-cholesten-3-one (Figures 1C and 5A).

Characterization of the two single point mutants, CYP125A3 W83Y and CYP125A4 Y87W, resulted in a partial reversal of each enzyme's substrate profile. CYP125A3 W83Y had drastically reduced activity toward 4-cholesten-3-one (K_M = 24.1 ± 7.8 μM; V_{max} = 0.02 ± 0.01 min^{-1}) (Figure 5A), with rates lower than that of WT CYP125A4, while the CYP125A4 Y87W mutant showed increased activity toward 4-cholesten-3-one (S_{50} = 28.3 ± 3.4 μM; n = 1.9 ± 0.3) (Figure 5A), albeit with sigmoidal kinetics. For 7α-hydroxy-4-cholesten-3-one, CYP125A4 Y87W showed greatly reduced activity relative to
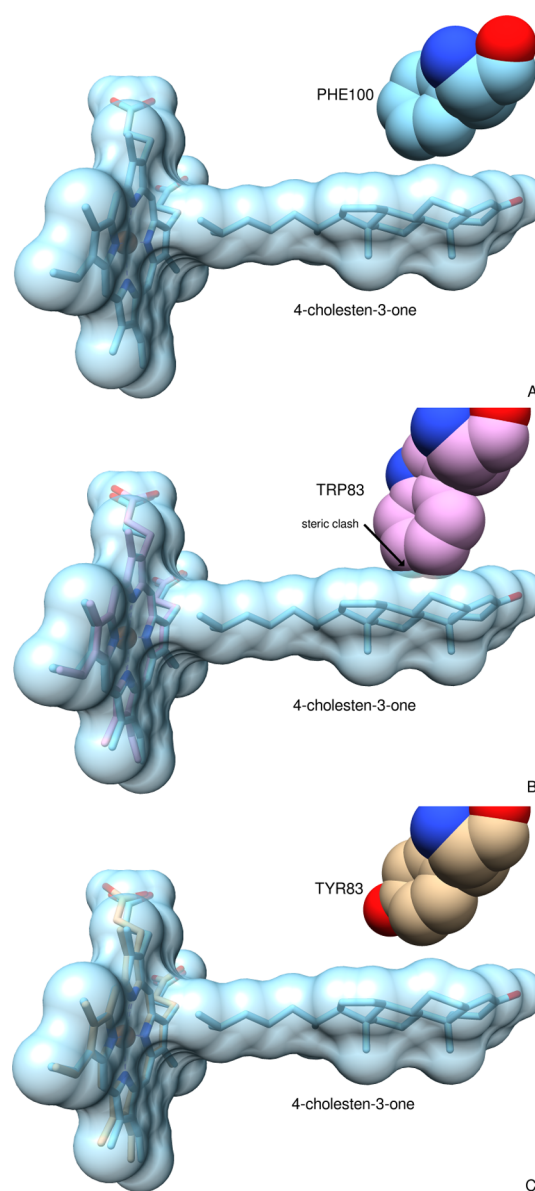

Figure 2. Aligned binding pockets of (A) CYP125A1 (2X5W), (B) wild-type CYP125A3 (4APY), and (C) CYP125A3 W83Y (5DQN). The 4-cholesten-3-one ligand (blue) is shown overlaid into the CYP125A3 active sites, showing steric clashes with Trp83 in the wild type (B) and elimination of clashes in the W83Y mutant (C).

the WT enzyme (K_M = 5.1 ± 1.3 μM; V_{max} = 0.16 ± 0.01 min^{-1}) (Figure 5B), while CYP125A3 W83Y showed low activity with small amounts of product being formed after incubation with this substrate for 90 min as well as with 7α-hydroxy-4-cholesten-3-one (Figure 5C).

CYP125A1, the primary cholesterol 26-hydroxylase in *Mtb*, also catalyzes the 26-hydroxylation of 7α-hydroxy-4-cholesten-3-one (Figure 5D). This is consistent with the crystal structure of the complex of 4-cholesten-3-one with the protein,[6] which reveals a cavity in the structure that could readily accommodate a 7α-hydroxy substituent (Figure 2A).

Taken together, these results show the critical role of a single residue, Trp or Tyr, in determining the alternate substrate profiles of the two CYP125 enzymes encoded in the *Msmeg* genome, and how these closely related enzymes have
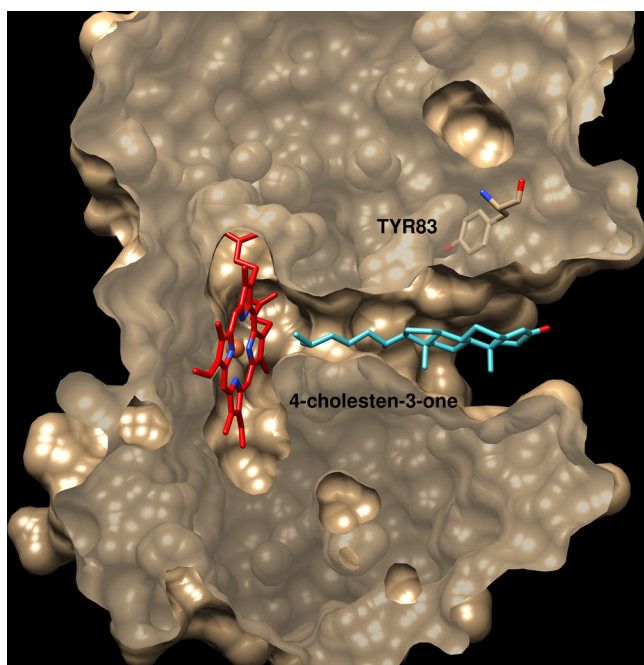
Figure 3. Cross-sectional view of the substrate access channel of CYP125A3 W83Y (5DQN) with 4-cholesten-3-one colored cyan and heme colored red. Generated using UCSF Chimera.[31,32]

overlapping yet distinct and complementary functions in this mycobacterial species.

■ DISCUSSION

The degradation of cholesterol and 4-cholesten-3-one is catalyzed in *Mtb* by both CYP125A1 and CYP142A1.[8] However, we recently reported that the structures of CYP142 enzymes, which have an uncapped active site, allow them also to oxidize cholesterol esters, whereas CYP125 enzymes, which have a capped active site, cannot catalyze this oxidation.[34] A similar difference exists between CYP125A3 and CYP142A2, the previously reported orthologs from *Msmeg*. In contrast to *Mtb*, deletion of these two enzymes impaired, but did not fully prevent, *in vitro* growth of *Msmeg* on cholesterol as the sole carbon source.[14] This implies the existence of an alternative pathway for cholesterol utilization. On the basis of its upregulation in response to cholesterol, CYP189A1 was first examined to determine if it had the required cholesterol metabolizing activity. However, our biochemical studies demonstrated that neither cholesterol nor 4-cholesten-3-one is a substrate for this enzyme. Our attention therefore turned to CYP125A4, a second CYP125 enzyme from *Msmeg*. As reported here, this enzyme has low cholesterol oxidizing activity in addition to a much stronger ability to oxidize sterols with a C-7 substituent. CYP125A4 thus broadens the ability of *Msmeg*, an environmental mycobacterium, to utilize diverse sterol substrates as carbon sources.

The structural constraints that control the ability to oxidize 7α-hydroxycholesterol have been investigated by comparing the protein sequences and activities of two members of the CYP125 family, CYP125A3, which readily oxidizes cholesterol but has very low activity for 7α-hydroxycholesterol, and CYP125A4, which strongly favors oxidation of 7α-hydroxycholesterol over that of cholesterol. Homology modeling suggested the presence of a bulky tryptophan rather than a tyrosine (or the phenylalanine of CYP125A1) at a position adjacent to C-7 of the sterol in the substrate−protein complex is largely responsible for the weakened ability of CYP125A3 to oxidize 7α-hydroxycholesterol. Generation of the CYP125A3 W83Y and CYP125A4 Y87W mutants confirmed the importance of this residue by partially reversing the substrate specificity for each enzyme (Figure 5), and structural comparison of CYP125A3 wild-type and mutant active sites
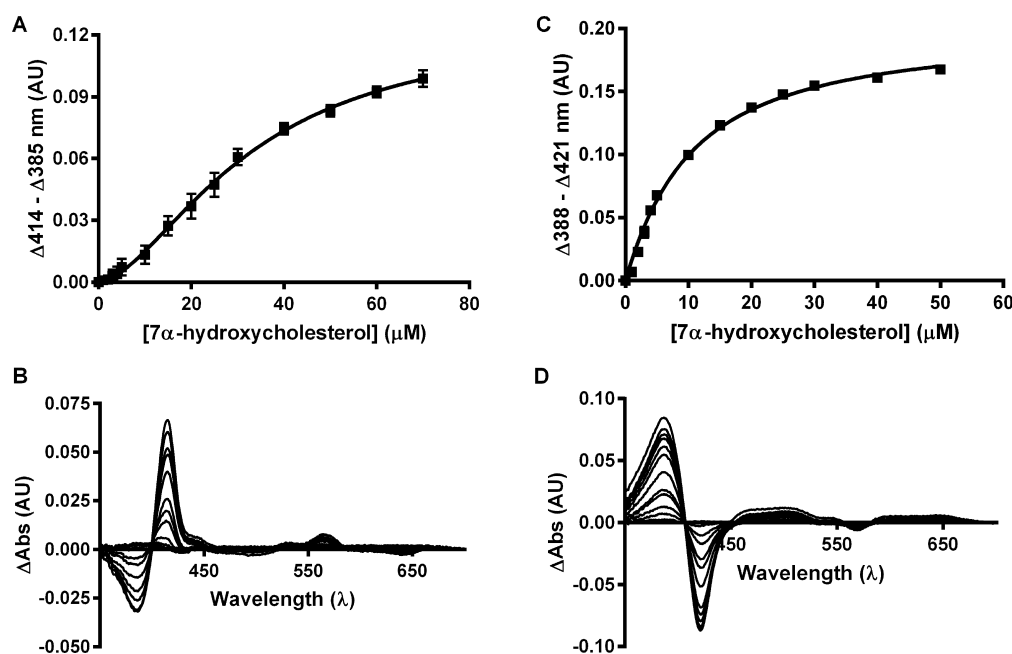

Figure 4. (A) Hill equation fit of (B) UV−visible spectroscopic changes induced by 7α-hydroxycholesterol binding to CYP125A3 (S_{50} = 32.9 ± 4.7 μM; n = 1.7 ± 0.2) and (C) quadratic binding equation fit of (D) UV−visible spectroscopic changes induced by 7α-hydroxycholesterol binding to CYP125A4 (K_S = 8.7 ± 0.5 μM).
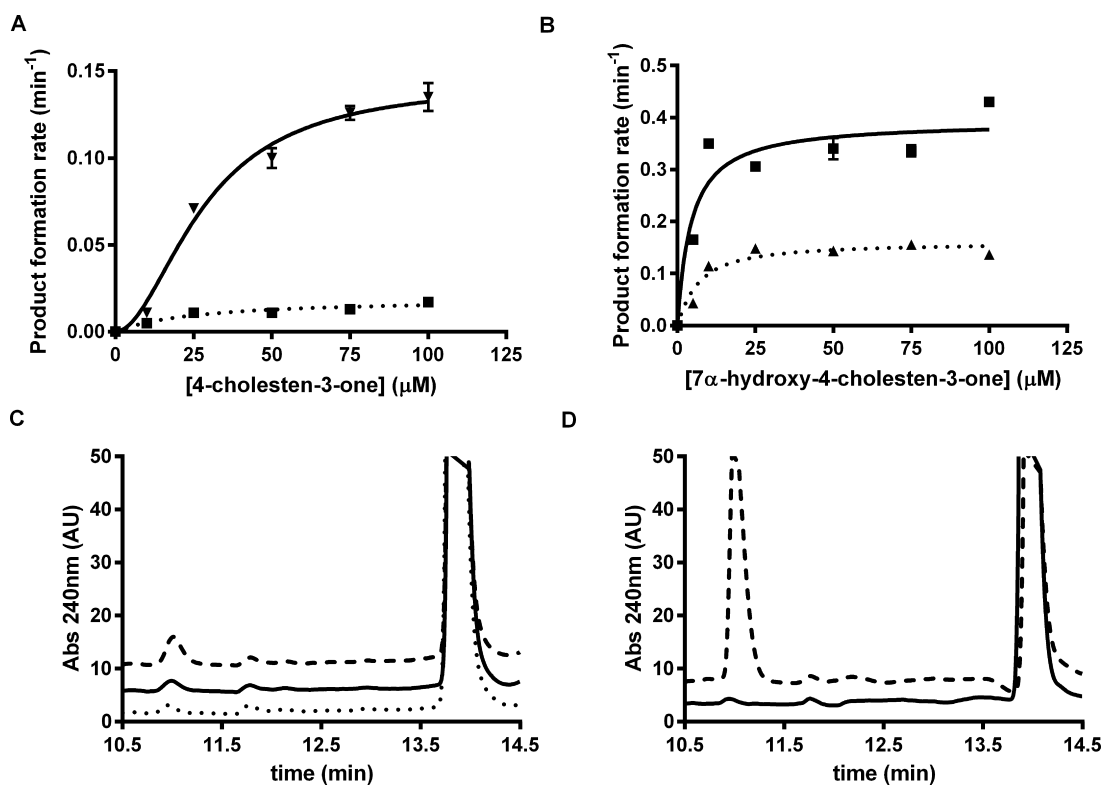
Figure 5. Fits of (A) 4-cholesten-3-one oxidation by CYP125A3 W83Y (solid line; k_{cat}/K_M = 0.01 μM^{-1} s^{-1}) and CYP125A4 Y87W (dashed line; k_{cat}/K_M = 0.001 μM^{-1} s^{-1}) and (B) 7α-hydroxy-4-cholesten-3-one oxidation by CYP125A4 (solid line; k_{cat}/K_M = 0.19 μM^{-1} s^{-1}) and CYP125A4 Y87W (dashed line; k_{cat}/K_M = 0.011 μM^{-1} s^{-1}). HPLC traces of 7α-hydroxy-4-cholesten-3-one oxidation by (C) CYP125A3 at the 0 min time point (small dashes) and 90 min time point (solid line) and CYP125A3 W83Y at the 90 min time point (large dashes) and (D) CYP125A1 at the 0 min time point (solid line) and 90 min time point (dashed line). The 10.7 min peak is the product 7α,26-dihydroxy-4-cholesten-3-one, and the substrate peak, 7α-hydroxy-4-cholesten-3-one, is at 14 min.

(Figure 2), which revealed a steric block preventing access for the substrate in the wild-type structure.

There are no obvious additional biological implications of the ability of CYP125A4 in *Msmeg* to oxidize 7α-hydroxycholesterol. However, the same is not true in *Mtb*, as 26-hydroxylation of 7α-hydroxycholesterol yields 7α,26-dihydroxycholesterol, a molecule that is a potent modulator of the host immune system.[16,17] These results suggest that there may be a signaling interaction between *Mtb* and its human host that impacts the pathogenicity of the mycobacterium. The reality of such an interaction will depend on the concentration of 7α-hydroxycholesterol available to the mycobacterium and the extent to which it exports the 7α,26-dihydroxycholesterol metabolite once it is formed.

The metabolism of cholesterol by *Mtb* has been linked to virulence of infection[1] and has been suggested as a target pathway for therapeutics.[7] While *Msmeg*, which has been used as a model system for understanding *Mtb*, shares a similar cholesterol metabolic pathway with its mycobacterial relative, this study illustrates subtle differences in the way these two species have adapted to respond to cholesterol. These differences must be considered when evaluating antimycobacterial compounds that target the cholesterol metabolizing pathway.

■ ASSOCIATED CONTENT

Accession Codes

CYP125A3 W83Y deposited as PDB entry 5DQN.

■ AUTHOR INFORMATION

Corresponding Author

*University of California, San Francisco, 600 16th St., N576D, San Francisco, CA 94158-2517. Telephone: +1 425 476-2903. E-mail: Ortiz@cgl.ucsf.edu.

ABBREVIATIONS

Mtb, M. tuberculosis; CYP, cytochrome P450; *Msmeg, M. smegmatis.*

REFERENCES

(1) Pandey, A. K., and Sassetti, C. M. (2008) Mycobacterial persistence requires the utilization of host cholesterol. *Proc. Natl. Acad. Sci. U. S. A. 105*, 4376−4380.

(2) Russell, D. G. (2001) *Mycobacterium tuberculosis*: here today, and here tomorrow. *Nat. Rev. Mol. Cell Biol. 2*, 569−577.

(3) Chang, J. C., Miner, M. D., Pandey, A. K., Gill, W. P., Harik, N. S., Sassetti, C. M., and Sherman, D. R. (2009) igr Genes and *Mycobacterium tuberculosis* cholesterol metabolism. *J. Bacteriol. 191*, 5232−5239.

(4) Yam, K. C., D'Angelo, I., Kalscheuer, R., Zhu, H., Wang, J. X., Snieckus, V., Ly, L. H., Converse, P. J., Jacobs, W. R., Jr., Strynadka, N., and Eltis, L. D. (2009) Studies of a ring-cleaving dioxygenase illuminate the role of cholesterol metabolism in the pathogenesis of *Mycobacterium tuberculosis. PLoS Pathog. 5*, e1000344.

(5) Griffin, J. E., Pandey, A. K., Gilmore, S. A., Mizrahi, V., McKinney, J. D., Bertozzi, C. R., and Sassetti, C. M. (2012) Cholesterol catabolism by *Mycobacterium tuberculosis* requires transcriptional and metabolic adaptations. *Chem. Biol. 19*, 218−227.

(6) Ouellet, H., Guan, S., Johnston, J. B., Chow, E. D., Kells, P. M., Burlingame, A. L., Cox, J. S., Podust, L. M., and Ortiz de Montellano, P. R. (2010) *Mycobacterium tuberculosis* CYP125A1, a steroid C27 monooxygenase that detoxifies intracellularly generated cholest-4-en-3-one. *Mol. Microbiol. 77*, 730−742.

(7) Ouellet, H., Johnston, J. B., and Ortiz de Montellano, P. R. (2011) Cholesterol catabolism as a therapeutic target in *Mycobacterium tuberculosis. Trends Microbiol. 19*, 530−539.

(8) Ouellet, H., Johnston, J. B., and Ortiz de Montellano, P. R. (2010) The *Mycobacterium tuberculosis* cytochrome P450 system. *Arch. Biochem. Biophys. 493*, 82−95.

(9) McLean, K. J., Belcher, J., Driscoll, M. D., Fernandez, C. C., Le Van, D., Bui, S., Golovanova, M., and Munro, A. W. (2010) The *Mycobacterium tuberculosis* cytochromes P450: physiology, biochemistry & molecular intervention. *Future Med. Chem. 2*, 1339−1353.

(10) Rosloniec, K. Z., Wilbrink, M. H., Capyk, J. K., Mohn, W. W., Ostendorf, M., van der Geize, R., Dijkhuizen, L., and Eltis, L. D. (2009) Cytochrome P450 125 (CYP125) catalyses C26-hydroxylation to initiate sterol side-chain degradation in *Rhodococcus jostii* RHA1. *Mol. Microbiol. 74*, 1031−1043.

(11) Garcia-Fernandez, E., Medrano, F. J., Galan, B., and Garcia, J. L. (2014) Deciphering the transcriptional regulation of cholesterol catabolic pathway in mycobacteria: identification of the inducer of KstR repressor. *J. Biol. Chem. 289*, 17576−17588.

(12) Kendall, S. L., Burgess, P., Balhana, R., Withers, M., Ten Bokum, A., Lott, J. S., Gao, C., Uhia-Castro, I., and Stoker, N. G. (2010) Cholesterol utilization in mycobacteria is controlled by two TetR-type transcriptional regulators: kstR and kstR2. *Microbiology 156*, 1362−1371.

(13) Kendall, S. L., Withers, M., Soffair, C. N., Moreland, N. J., Gurcha, S., Sidders, B., Frita, R., Ten Bokum, A., Besra, G. S., Lott, J. S., and Stoker, N. G. (2007) A highly conserved transcriptional repressor controls a large regulon involved in lipid degradation in *Mycobacterium smegmatis* and *Mycobacterium tuberculosis. Mol. Microbiol. 65*, 684−699.

(14) Garcia-Fernandez, E., Frank, D. J., Galan, B., Kells, P. M., Podust, L. M., Garcia, J. L., and Ortiz de Montellano, P. R. (2013) A highly conserved mycobacterial cholesterol catabolic pathway. *Environ. Microbiol. 15*, 2342−2359.

(15) Uhia, I., Galan, B., Kendall, S. L., Stoker, N. G., and Garcia, J. L. (2012) Cholesterol metabolism in *Mycobacterium smegmatis. Environ. Microbiol. Rep. 4*, 168−182.

(16) Liu, C., Yang, X. V., Wu, J., Kuei, C., Mani, N. S., Zhang, L., Yu, J., Sutton, S. W., Qin, N., Banie, H., Karlsson, L., Sun, S., and Lovenberg, T. W. (2011) Oxysterols direct B-cell migration through EBI2. *Nature 475*, 519−523.

(17) Hannedouche, S., Zhang, J., Yi, T., Shen, W., Nguyen, D., Pereira, J. P., Guerini, D., Baumgarten, B. U., Roggo, S., Wen, B., Knochenmuss, R., Noel, S., Gessier, F., Kelly, L. M., Vanek, M., Laurent, S., Preuss, I., Miault, C., Christen, I., Karuna, R., Li, W., Koo, D. I., Suply, T., Schmedt, C., Peters, E. C., Falchetto, R., Katopodis, A., Spanka, C., Roy, M. O., Detheux, M., Chen, Y. A., Schultz, P. G., Cho, C. Y., Seuwen, K., Cyster, J. G., and Sailer, A. W. (2011) Oxysterols direct immune cell migration via EBI2. *Nature 475*, 524−527.

(18) Barnes, H. J., Arlotto, M. P., and Waterman, M. R. (1991) Expression and enzymatic activity of recombinant cytochrome P450 17 alpha-hydroxylase in *Escherichia coli. Proc. Natl. Acad. Sci. U. S. A. 88*, 5597−5601.

(19) Ouellet, H., Lang, J., Couture, M., and Ortiz de Montellano, P. R. (2009) Reaction of *Mycobacterium tuberculosis* cytochrome P450 enzymes with nitric oxide. *Biochemistry 48*, 863−872.

(20) Yasukawa, T., Kanei-Ishii, C., Maekawa, T., Fujimoto, J., Yamamoto, T., and Ishii, S. (1995) Increase of solubility of foreign proteins in *Escherichia coli* by coproduction of the bacterial thioredoxin. *J. Biol. Chem. 270*, 25328−25331.

(21) Omura, T., and Sato, R. (1964) The carbon monoxide-binding pigment of liver microsomes. II. Solubilization, purification, and properties. *J. Biol. Chem. 239*, 2379−2385.

(22) Eswar, N., Webb, B., Marti-Renom, M. A., Madhusudhan, M. S., Eramian, D., Shen, M. Y., Pieper, U., and Sali, A. (2007) Comparative protein structure modeling using MODELLER. *Current Protocols in Protein Science*, Chapter 2, Unit 2.9, Wiley, New York.

(23) Holton, J., and Alber, T. (2004) Automated protein crystal structure determination using ELVES. *Proc. Natl. Acad. Sci. U. S. A. 101*, 1537−1542.

(24) Leslie, A. G. W., Brick, P., and Wonacott, A. (1986) *Daresbury Laboratory Information Quarterly for Protein Crystallography*, Vol. 18, pp 33−39, Daresbury Laboratory, Warrington, U.K.

(25) Steller, I., Bolotovsky, R., and Rossmann, M. G. (1997) An Algorithm for Automatic Indexing of Oscillation Images using Fourier Analysis. *J. Appl. Crystallogr. 30*, 1036−1040.

(26) Collaborative Computational Project, Number 4 (1994) The CCP4 suite: programs for protein crystallography. *Acta Crystallogr., Sect. D: Biol. Crystallogr. 50*, 760−763.

(27) Adams, P. D., Afonine, P. V., Bunkoczi, G., Chen, V. B., Davis, I. W., Echols, N., Headd, J. J., Hung, L. W., Kapral, G. J., Grosse-Kunstleve, R. W., McCoy, A. J., Moriarty, N. W., Oeffner, R., Read, R. J., Richardson, D. C., Richardson, J. S., Terwilliger, T. C., and Zwart, P. H. (2010) PHENIX: a comprehensive Python-based system for macromolecular structure solution. *Acta Crystallogr., Sect. D: Biol. Crystallogr. 66*, 213−221.

(28) Painter, J., and Merritt, E. A. (2006) Optimal description of a protein structure in terms of multiple groups undergoing TLS motion. *Acta Crystallogr., Sect. D: Biol. Crystallogr. 62*, 439−450.

(29) Voss, N. R., and Gerstein, M. (2010) 3V: cavity, channel and cleft volume calculator and extractor. *Nucleic Acids Res. 38*, W555−562.

(30) Darby, N. J., and Creighton, T. E. (1993) *Protein structure: In focus 97*. Oxford University Press, Oxford.

(31) Meng, E. C., Pettersen, E. F., Couch, G. S., Huang, C. C., and Ferrin, T. E. (2006) Tools for integrated sequence-structure analysis with UCSF Chimera. *BMC Bioinf. 7*, 339.

(32) Pettersen, E. F., Goddard, T. D., Huang, C. C., Couch, G. S., Greenblatt, D. M., Meng, E. C., and Ferrin, T. E. (2004) UCSF Chimera–a visualization system for exploratory research and analysis. *J. Comput. Chem. 25*, 1605−1612.

(33) Sanner, M. F., Olson, A. J., and Spehner, J. C. (1996) Reduced surface: an efficient way to compute molecular surfaces. *Biopolymers 38*, 305−320.

(34) Frank, D. J., Madrona, Y., and Ortiz de Montellano, P. R. (2014) Cholesterol ester oxidation by mycobacterial cytochrome P450. *J. Biol. Chem. 289*, 30417−30425.